Journal of Electronics, Electromedical Engineering, and Medical Informatics
Homepage: jeeemi.org; Vol. 8, No. 2, April 2026, pp: 657-671 e-ISSN: 2656-8632

RESEARCH ARTICLE OPEN ACCESS

LRSE-LCC: A Lightweight Residual CNN with Squeeze-and-Excitation Attention for Lung Cancer Classification from CT Image

Dhaval J. Rana[1] and Keyur Rana[2]

[1] Department of Computer Engineering, Gujarat Technological University, Gujarat, India
[2] Department of Computer Engineering, Sarvajanik College of Engineering and Technology-SCET, Gujarat, India

Corresponding author: Dhaval J. Rana (e-mail: djr.fetr@gmail.com), **Author Email**: Keyur Rana (e-mail: keyur.rana@scet.ac.in)

Abstract: Lung cancer is still a major cause of cancer deaths globally, and there is a need for accurate and early diagnostic systems. Although deep learning models have shown encouraging results in classifying lung cancer from CT scans, most are computationally complex. This paper proposes the design of a lightweight and accurate deep learning model for multi-class lung cancer classification from CT scans. A new model called Lightweight Residual CNN with Squeeze-and-Excitation Lung Cancer Classification (LRSE-LCC) is proposed. The model combines lightweight residual learning for stable gradient flow and channel attention for improved feature representation. Dual global pooling is used by combining Global Average Pooling and Global Max Pooling to enable complementary feature extraction. In addition, a balanced batch training method is used to handle class imbalance. The proposed model was tested on the IQ-OTH/NCCD lung CT image dataset, which includes normal, benign, and malignant images. Image resizing and normalization were done before training. The proposed LRSE-LCC model achieved a test accuracy of 98.19%. Sensitivity was 100.00%, indicating strong ability to detect malignant images. The model achieved a specificity of 99.04%, reducing false-positive predictions. The macro-averaged AUC was 99.90%. The AUC values for all classes exceeded 99.80%, indicating outstanding classification performance. The macro F1-score was 96.42%. The value of the Cohen's kappa coefficient was 96.88%, which ensured that the agreement was not by chance. The overall error rate was limited to 1.81%. In conclusion, the proposed LRSE-LCC model has both high classification accuracy and efficiency. The combination of residual learning, channel attention, and dual pooling helps to greatly improve the accuracy of multi-class diagnosis. The proposed lightweight model has great potential for application in real-world computer-aided lung cancer diagnosis systems.

Keywords **Lung cancer classification, Computed tomography, Residual CNN, Squeeze-and-Excitation, Deep learning, Medical image analysis**

I. Introduction

Lung cancer remains one of the most dangerous and deadly diseases globally, contributing significantly to cancer-related mortality. The American Cancer Society estimated that in 2024, there were roughly 2,34,580 new cases and 1,25,070 fatalities due to lung cancer in the USA [1]. Globally, lung cancer accounted for over 2.48 million new cases and 1.82 million fatalities in 2022 [2], making it the leading cause of cancer-related mortality [3][4]. Deep learning, specifically CNNs (convolutional neural networks), has demonstrated a very good results in automated medical image processing in recent years [5], including the detection and categorization of lung cancer [6]. Recent multi-scale residual network frameworks have further improved diagnostic accuracy for pulmonary nodules on CT images [7]. CNN-based methods can reduce the need for handcrafted features by directly learning hierarchical feature representations from CT images [8]. Despite these advantages, a lot of current techniques rely on extremely complex and parameter-intensive architectures like DenseNet, and EfficientNet. These architectures were first created for massive datasets of natural images [9][10][11].

Many popular deep learning architectures in the field of medical image analysis, such as ResNet50 (~25M parameters), DenseNet121 (~8M parameters), and the EfficientNet family (~5-30M parameters), are computationally expensive and memory-intensive. These models typically require powerful computing hardware to run. Furthermore, these types of models may face the problem of overfitting and poor

Manuscript received 13 February 2026; Revised 10 April 2026; Accepted 12 April 2026; Available online 18 April 2026
Digital Object Identifier (**DOI**): https://doi.org/10.35882/jeeemi.v8i2.1574

generalization when working with small and unbalanced datasets in the field of medical image analysis [12]. Beyond mortality statistics, early diagnosis and structured screening strategies remain fundamental to reducing lung cancer–related deaths and improving patient prognosis [13].

Several studies have proposed CNN-based models with different strategies to enhance the accuracy of diagnosis [14]. Optimization-based models have also been extensively investigated, such as CNN models coupled with metaheuristic optimization techniques like Snake Optimization [15] and the AlexNet model optimized using Bowerbird optimization [16]. Ensemble CNN models have also been found to possess high accuracy and robustness even on small-sized datasets [17]. Recent ensemble-based ResNet architectures have demonstrated improved malignant–benign discrimination performance on CT images [18]. Segmentation-based approaches have also made great progress in model performance [19]. The UDCT model integrated a modified U-Net with Differentiable Architecture Search (DARTS) and multi-level Otsu thresholding, and obtained competitive results [20]. YOLOv8 (anchor-based) and Mask R-CNN (anchor-free) detectors achieved better precision and recall by applying an attention mechanism to lung nodule segmentation [21]. These approaches show the key role of segmentation in enhancing the reliability of classification. More recently, advanced deep learning strategies incorporating temporal and longitudinal information have been explored to enhance malignancy prediction in screen-detected lung nodules [22]. Transfer learning has been another important area. MobileNetV2 transfer learning with stacked GRU layers and Grad-CAM explainability achieved the best prediction results [23]. GoogLeNet transfer learning also demonstrated substantial enhancement in prediction accuracy [24], and hybrid transfer learning frameworks such as VER-Net have further improved lung cancer detection performance on CT datasets [25]. Other CNN-based models, such as AlexNet [26] and Google AI Studio model [27], achieved competitive results but have some drawbacks in classifying benign and malignant cases.

Conventional machine learning techniques, such as SVM with manual feature extraction, achieved moderate accuracy [28], thereby confirming the relative superiority of deep learning. Other hybrid and feature-engineered models, like AlexNet with Gabor wavelet and GLCM features [16], as well as weakly supervised and attention-based learning [14][30][31][32][33][34][22][29], further substantiate the diversity of approaches developed in this area. Recently, multi-scale transformer-based architectures such as MSM-ViT have been proposed for pulmonary nodule classification on CT images, demonstrating competitive performance compared to conventional CNN-based approaches [35]. Ensemble-based deep learning frameworks have also been proposed to enhance robustness and generalization in lung cancer detection tasks [36]. Recently, capsule-network–based architectures have also been explored for lung cancer classification on CT images, demonstrating enhanced feature representation capabilities [37]. However, despite these developments, many of the existing models are still computationally expensive or rely on extensive pre-processing, which makes them less applicable in real-time clinical settings. Furthermore, although attention mechanisms have been explored in segmentation models, their incorporation into lightweight CNN classifiers for direct lung cancer classification remains underdeveloped.

To improve feature representation, CNN architectures can utilize attention mechanisms to focus on informative features while ignoring irrelevant ones. The capability of the Squeeze-and-Excitation (SE) attention mechanism to recalibrate features at the channel level has made it unique among the others [38]. However, the integration of SE attention into the network often results in more complex structures, which limit the applicability of the models in practical implementations due to resource constraints. Moreover, the majority of the current approaches to lung cancer classification only employ a single global pooling method to aggregate the features and have not addressed the issue of class imbalance, which may significantly affect the reliability of the diagnosis. To overcome the limitations of the current classification methods for lung cancer, such as high computational complexity and poor sensitivity to subtle CT image features, this paper proposes LRSE-LCC, a lightweight residual CNN with SE attention. In this context, the term "lightweight" refers to a model architecture with fewer trainable parameters, a simpler structure, and efficient mechanisms for feature learning. The LRSE-LCC model that we propose has approximately 1.29M parameters, which is much fewer compared to other traditional deep CNN architectures. This is due to the use of compact residual blocks and efficient channel attention mechanisms. The proposed LRSE-LCC model combines compact residual learning and channel-wise attention with dual global pooling for efficient and effective feature discrimination, and it can be used in clinical decision support systems. The key contributions of this work are summarized as follows:

1. A **lightweight residual CNN with embedded SE attention (**LRSE-LCC**)** is proposed to improve channel-wise feature recalibration and stable gradient propagation without relying on deep or parameter-heavy architectures.
2. A **dual global feature aggregation strategy** using Global Average Pooling (GAP) and Global

Manuscript received 13 February 2026; Revised 10 April 2026; Accepted 12 April 2026; Available online 18 April 2026
Digital Object Identifier (**DOI**): https://doi.org/10.35882/jeeemi.v8i2.1574

Max Pooling (GMP) is employed to capture complementary global contextual and salient lesion information.
3. A **balanced batch training scheme** is implemented to handle class imbalance and improve model robustness.
4. The proposed LRSE-LCC model is evaluated using the "IQ-OTH/NCCD" lung cancer dataset [39]. It achieved superior performance in multi-class lung cancer classification.

The rest of the paper is organized as follows: In Section II, the dataset description/preprocessing, balanced batch construction, training configuration, and the model architecture are discussed. In Section III, the results are presented along with the performance evaluation. In Section IV, the performance is compared with state-of-the-art techniques, while the conclusion is presented in Section V.

II. Methods

A. Dataset Description

The experiments were conducted on the "IQ-OTH/NCCD" lung cancer dataset. It is a publicly available benchmark dataset. It is developed by two specialized oncology institutions in Iraq. The dataset, introduced in 2019, comprises thoracic CT images collected from individuals diagnosed with lung cancer at different stages, along with scans from healthy subjects. This dataset includes 1,100 CT images. It contains the various anatomical levels of the chest. Based on professional clinical diagnosis, images are divided into three classes: benign, malignant, and normal. The dataset was partitioned into training, validation, and test subsets using a 70:15:15 ratio. Accordingly, 70% of the samples were allocated to model training, 15% to validation, and the remaining 15% to independent performance evaluation. The test subset remained entirely unseen throughout the model development process. Each of these images was thoroughly annotated and individually validated by experienced radiologists and oncologists from respective hospitals. The study has obtained ethical approval from the institutional review boards of the respective medical centers involved in the study. The dataset was provided in an anonymized fashion for research purposes. The dataset represents a wide spectrum of patients, including variations in their ages, genders, living conditions, educational backgrounds, and geographic origins. Some of the representative images of CT scans from the "IQ-OTH/NCCD" dataset are shown in Fig. 1. and include images from normal, benign, and malignant cases.

(a) **(b)** **(c)**

Fig. 1. Representative CT Images from "IQ-OTH/NCCD" dataset (a) malignant**, (b)** benign**, (c)** normal [39]

B. Data Preprocessing

All the CT images are resized to a fixed resolution of 224 × 224 pixels. The resolution of 224 × 224 was selected as it provides a balance between preserving important anatomical details and maintaining computational efficiency. It is also a commonly used input size in CNN-based architectures, enabling stable training and efficient processing. However, it is acknowledged that resizing may lead to the loss of fine-grained details in very small lesions, which remains a potential limitation. Then, the grayscale CT images are converted to a three-channel image representation to maintain compatibility with standard CNN design practices. Since CT images are inherently grayscale, the single-channel data are replicated across three channels. This does not introduce additional information but ensures compatibility with conventional convolutional frameworks. However, using a single-channel input could also reduce the computational

Manuscript received 13 February 2026; Revised 10 April 2026; Accepted 12 April 2026; Available online 18 April 2026
Digital Object Identifier (**DOI**): https://doi.org/10.35882/jeeemi.v8i2.1574

cost. The three-channel configuration was chosen to ensure stable training behaviour. Investigating the single-channel input to reduce the computational cost without affecting performance is a potential future work. To improve numerical stability and facilitate faster and more stable convergence during training, the pixel values are normalized to the range [0, 1] [40] by dividing by 255. This preprocessing pipeline standardizes the input data and preserves relevant anatomical and pathological information. As a result, the network can focus on learning discriminative lung features rather than compensating for variations in image scale or intensity distribution. No explicit data augmentation techniques were applied in this study. The preprocessing pipeline is limited to resizing, channel conversion, and normalization.

C. Balanced Batch Construction

The "IQ-OTH/NCCD" dataset has a large-scale class imbalance between normal, benign and malignant CT images. To overcome this issue and improve the representation of all three classes, a custom balanced batch generation technique is used during training. Instead of using random sampling at each mini batch, an equal number of samples from each class is used. For a batch size of 12, 4 images from each class are used at each training step. This approach also makes sure that all classes are represented equally in the loss function and gradient updates, which in turn improves training stability and also increases the model's performance on the smaller class samples. The sampling process is performed with replacement to ensure continuous availability of samples from all classes during training. Each epoch is defined using a fixed number of training steps to maintain stable training dynamics. This strategy ensures consistent class balance across batches and improves model

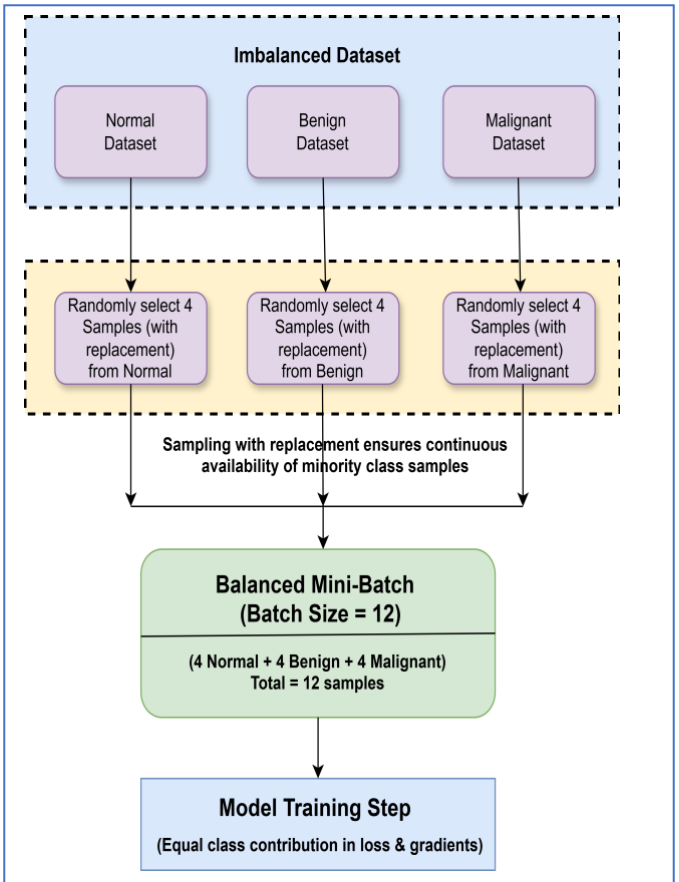

Fig. 2. Balanced batch construction with equal sampling (with replacement) from normal, benign, and malignant classes.

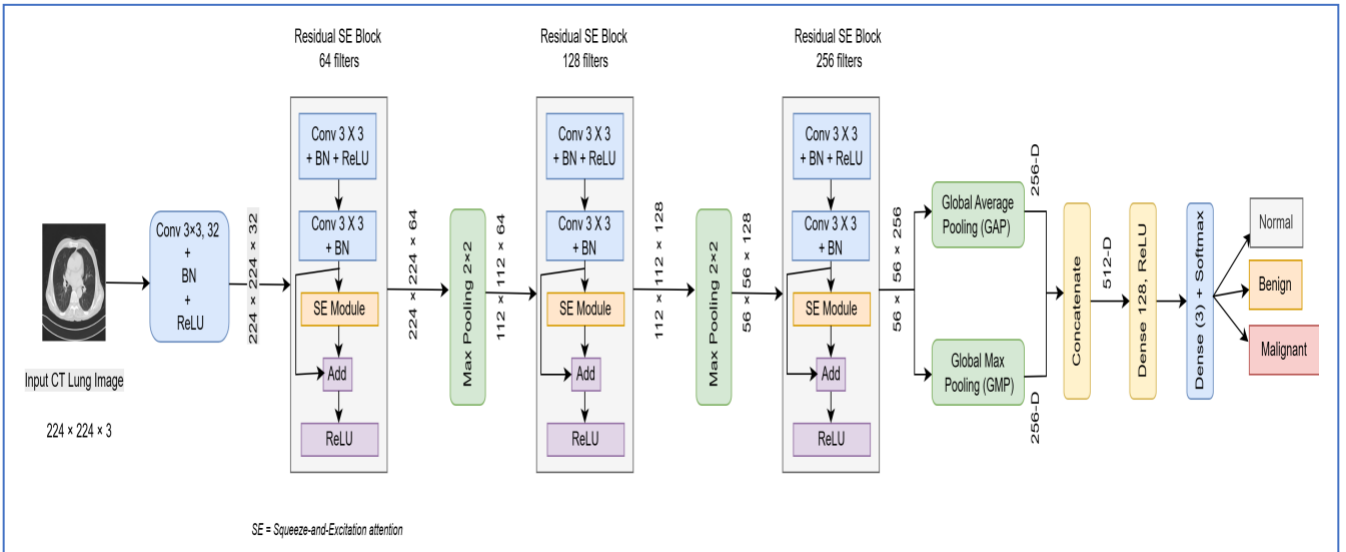

Fig. 3. Architecture of the proposed LRSE-LCC lightweight residual CNN with squeeze-and-excitation attention for lung cancer classification.

Manuscript received 13 February 2026; Revised 10 April 2026; Accepted 12 April 2026; Available online 18 April 2026
Digital Object Identifier (**DOI**): https://doi.org/10.35882/jeeemi.v8i2.1574

Algorithm 1. Proposed LRSE-LCC Framework

Input: CT lung images
Output: Class label ∈ {Normal, Benign, Malignant}
Acquire CT lung images
Normalize intensities to [0,1] and resize images to 224 × 224 × 3.
Divide the dataset into test, validation, and training sets.
Initialize the proposed LRSE-LCC network
Extract initial features using Conv(3×3, 32) + BN + ReLU
For Residual-SE blocks k = {64, 128, 256} filters do
    Apply Conv → BN → ReLU → Conv → BN → SE attention → shortcut addition → ReLU
    Apply 2×2 max-pooling after the first and second blocks
End for
Apply GAP and GMP in parallel
Concatenate pooled features
Apply Dense(128) + ReLU
Apply Softmax layer (3 classes)
Train the network using Adam optimizer and categorical cross-entropy loss
Validate during training and select the best model
Evaluate on the independent test set
Evaluate performance using Accuracy, Precision, Recall, F1-score, and Cohen's κ
Output predicted lung cancer class labels

robustness. A schematic illustration of the balanced batch construction process is shown in **Fig**. 2.

D. Proposed model Architecture

A lightweight residual CNN incorporating squeeze-and-excitation attention is introduced for CT-based lung cancer classification, and is termed LRSE-LCC. The architectural overview of the LRSE-LCC model is shown in Fig. 3. , and the step-by-step workflow of the proposed method is described in Algorithm 1. The model is designed to achieve an effective balance between representational power and computational efficiency by integrating residual learning and channel-wise attention mechanisms within a compact CNN framework. The model receives a CT lung image of dimension 224 × 224 × 3 as input. Feature extraction begins with a 3 × 3 convolutional layer comprising 32 filters, after which batch normalization and ReLU activation are applied. This initial stage extracts low-level structural patterns, such as edges and intensity variations, while stabilizing the training process. Later, the network consists of three consecutive Residual Squeeze-and-Excitation blocks with 64, 128, and 256 filters, respectively. The progressive increase in filter sizes follows standard CNN design principles, allowing the network to capture increasingly complex and high-level feature representations. These values were empirically selected to achieve a balance between classification performance and computational efficiency, thereby supporting the lightweight design of the proposed model. In each Residual Squeeze-and-Excitation block, there are two convolutional layers. The initial convolutional operation is subsequently normalized using batch normalization and activated through a ReLU function. In contrast, the second convolutional layer applies only batch normalization. The extracted feature maps are passed through a squeeze-and-excitation block, where channel weights are dynamically refined based on inter-channel correlations. The identity shortcut connection is applied to facilitate the effective gradient flow and avoid degradation in the deeper layers. When the number of channels changes, a 1 × 1 convolution is applied along the shortcut path to ensure dimensional consistency before element-wise addition. Finally, a ReLU activation function is applied to generate the block output.

After the first and second Residual-SE blocks, 2 × 2 max-pooling layers are applied. It is used to progressively reduce the spatial resolution while preserving the discriminative features. This hierarchical design allows our LRSE-LCC model to learn increasingly abstract and semantically meaningful representations relevant to lung lesion characterization. After the final Residual-SE block, GAP and GMP [41] layers are applied in parallel. The feature vectors obtained from these two pooling methods are concatenated to generate a combined feature vector. While GAP operation gathers global contextual information by taking the average of the spatial feature responses, GMP is focused on the most salient and discriminative feature activations in the feature maps. Thus, by combining GAP and GMP, this feature extraction mechanism is able to learn both global contextual and local feature information, which makes it more robust and discriminative compared to

Manuscript received 13 February 2026; Revised 10 April 2026; Accepted 12 April 2026; Available online 18 April 2026
Digital Object Identifier (**DOI**): https://doi.org/10.35882/jeeemi.v8i2.1574

using either pooling method individually. This hybrid pooling approach enhances the robustness of the learned representation without incurring substantial computational costs. The combined feature vector is then fed into a fully connected layer with 128 neurons and ReLU activation for high-level feature integration. The final classification layer comprises a softmax-activated dense layer with three outputs, representing normal, benign, and malignant classes. Overall, the proposed LRSE-LCC architecture combines residual learning, squeeze-and-excitation attention, and hybrid global pooling within a lightweight CNN design, enabling effective and stable training while enhancing discriminative feature learning for lung cancer classification. It has a low parameter count of approximately 1.29 million, making it computationally efficient compared to conventional deep CNN architectures. The lightweight nature of the proposed architecture is achieved by limiting the number of layers, using compact residual blocks, and incorporating efficient attention mechanisms without significantly increasing computational overhead.

E. Squeeze-and-Excitation Attention Mechanism

To improve the capability of the proposed LRSE-LCC model, a squeeze-and-excitation attention module is embedded within each residual block [38], as shown in **Fig. 4.** The SE module improves feature representation by adaptively adjusting channel importance based on relationships among feature maps.

Let the input feature map to the SE module be expressed as shown in Eq. (1) [38].

$$X \in \mathbb{R}^{H \times W \times C} \quad (1)$$

where H, W, and C represent the feature map height, width, and channel dimension, respectively.

1) Squeeze operation

In order to create a channel descriptor, the squeeze operation uses GAP to aggregate the spatial information of each channel, as expressed in Eq. (2) [38].

$$Z \in \mathbb{R}^{C} \quad (2)$$

Each element of z is computed as shown in Eq. (3) [38].

$$z_c = \frac{1}{H \times W} \sum_{i=1}^{H} \sum_{j=1}^{W} X_c(i,j), \; c = 1,2,\ldots,C \quad (3)$$

where Xc(i,j) denotes the activation at spatial location (i,j) of the c-th channel. Global spatial information is compressed into a small channel-wise representation via this procedure.

2) Excitation operation

The excitation operation is defined as shown in Eq. (4) [38]. It uses a gating mechanism made up of two fully connected layers to simulate inter-channel connections:

$$s = \sigma(W_2 \delta(W_1 z)), \quad (4)$$

$W_1 \in \mathbb{R}^{\frac{C}{r} \times C}$ and $W_2 \in \mathbb{R}^{C \times \frac{C}{r}}$ are learnable weight matrices of the excitation operation, where r denotes the reduction ratio, which is set to 16 in this study. The function $\delta(.)$ denotes the ReLU activation function, and $\sigma(.)$ represents the sigmoid activation function. The value of r is commonly used as it provides a balance between computational efficiency and the effectiveness of channel-wise feature recalibration. A smaller value of r increases computational cost, whereas a larger value may reduce the ability of the attention mechanism to capture channel interdependencies. The output $s \in \mathbb{R}^{C}$ contains normalized channel-wise attention coefficients.

3) Feature recalibration

Finally, the original feature maps are adaptively recalibrated via channel-wise multiplication, as expressed in Eq. (5) [38].

$$\tilde{X}_c = s_c * X_c, \quad c = 1,2,\ldots,C \quad (5)$$

where s_c denotes the attention weight associated with the c-th channel. This operation emphasizes informative feature channels and suppresses less relevant ones. The LRSE-LCC model is able to selectively enhance diagnostically meaningful channel responses, improve feature representation quality and classification performance with minimal additional computational cost by integrating this SE attention mechanism into each residual block.

Table 1. Hyper-parameters settings of the Proposed LRSE-LCC Model

Parameters	Value
Image size	224 × 224 × 3
Batch size	12
Optimizer	Adam
Learning rate	0.0001
Activation (output)	Softmax
Epochs	50
Normalization	Batch Normalization
Loss function	Categorical Cross-Entropy

F. Training Configuration

The LRSE-LCC model is trained on the "IQ-OTH/NCCD" lung CT dataset and is implemented using TensorFlow and Keras. The preprocessing pipeline resized all input CT images to 224 × 224 × 3 and

Manuscript received 13 February 2026; Revised 10 April 2026; Accepted 12 April 2026; Available online 18 April 2026
Digital Object Identifier (**DOI**): https://doi.org/10.35882/jeeemi.v8i2.1574

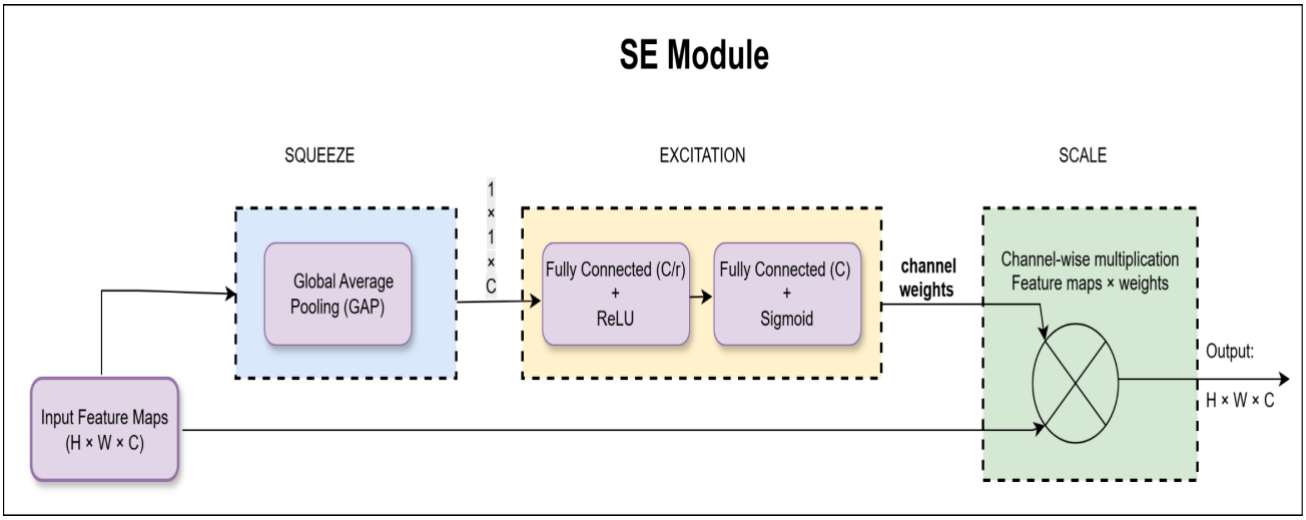

Fig. 4. Structure of the squeeze-and-excitation attention module illustrating squeeze, excitation, and channel-wise feature recalibration.

normalized them to the range [0, 1]. A custom balanced batch generator mitigated class imbalance by ensuring that each training batch contained equal numbers of samples from the normal, benign, and malignant classes. The training process used the Adam optimizer with categorical cross-entropy loss and a learning rate of 1×10^{-4}. The output layer employed SoftMax activation for three-class classification. Training was conducted for up to 50 epochs with a batch size of 12 for balanced training. Validation and testing were performed using standard Keras data generators with image rescaling. Table 1. provides a summary of the proposed LRSE-LCC model's comprehensive hyperparameter setup. Validation loss was monitored with a patience parameter of 8 epochs, enabling early stopping and restoration of the best-performing model weights. In addition, model checkpointing was used to save the network, achieving the highest validation accuracy. Model performance was finally evaluated on an independent test set using accuracy, classification metrics, ROC–AUC, and Cohen's kappa coefficient.

Table 2. Results of 5-Fold Cross-Validation for the LRSE-LCC Mode

Metric	Mean (%)	Std (%)
Accuracy	98.70	0.59
Macro F1-score	97.73	0.85
Benign Recall	92.79	4.57
Malignant Recall	100.00	0.00
Normal Recall	98.62	1.29
Cohen's Kappa	97.75	0.01

G. Cross- Validation Strategy

To ensure the robustness and stability of the proposed LRSE-LCC model, a stratified 5-fold cross-validation (CV) strategy [42] was performed on the training dataset. The training data were partitioned into 5 equal folds while preserving the class distribution across benign, malignant, and normal categories. Four folds were utilized for model training, and the remaining fold was used for validation in each iteration. Each fold was used as the validation set once, and this process was done five times.

The model architecture, training configuration, balanced batch generation strategy, and early stopping criteria were kept consistent across all folds to ensure a fair evaluation. Performance metrics, including accuracy, macro-averaged F1-score, recall (sensitivity), and Cohen's kappa coefficient, were computed for each fold. The mean ± standard deviation over the 5 folds was used to report the final cross-validation performance. An independent test set was not used during cross-validation and was reserved exclusively for final performance evaluation.

III. Result

To assess the robustness of the proposed LRSE-LCC model, a stratified 5-fold cross-validation was performed on the training dataset. The model achieved a mean accuracy of 98.70% with a low standard deviation of 0.59%, as shown in Table 2. The macro F1-score was 97.73%, while Cohen's kappa reached 97.75%, indicating excellent agreement between predicted and true labels. The recall values for malignant, normal, and benign cases were 100.00%, 98.62%, and 92.79%, respectively. The perfect recall for malignant cases highlights the model's strong

Manuscript received 13 February 2026; Revised 10 April 2026; Accepted 12 April 2026; Available online 18 April 2026
Digital Object Identifier (**DOI**): https://doi.org/10.35882/jeeemi.v8i2.1574

capability in detecting critical cancer cases, which is essential for clinical applications. The slightly lower recall for benign cases (92.79%) suggests minor confusion between benign and early malignant patterns, which is a known challenge in medical imaging.

Several evaluation parameters were used to assess the performance of the proposed LRSE-LCC model on the "IQ-OTH/NCCD" lung cancer CT imaging dataset. The accuracy curves of the training set and the validation set are shown in Fig. 5 (a). The accuracy of the training set rises rapidly and stabilizes, whereas the accuracy of the validation set has a similar trend, showing a stable learning curve and good generalization ability. The accuracy of the LRSE-LCC model on the training set, the validation set, and the final test set was 100%, 98.28%, and 98.19%, respectively. As shown in Fig. 5(b), the training and validation curves have a smooth declining trend with the increase of epoch numbers and remain steady at low levels, indicating that the optimization of the proposed architecture is efficient and there is no phenomenon of overfitting. The classification report indicates that the proposed model achieved high precision (99.00%) and recall (100.00%) for malignant cases, ensuring reliable detection of cancerous samples. Normal cases also achieved strong performance with recall values of 98.00%, while benign cases showed slightly lower recall (89.00%), primarily due to visual similarities between benign and malignant nodules [31]. These results highlight the model's strong

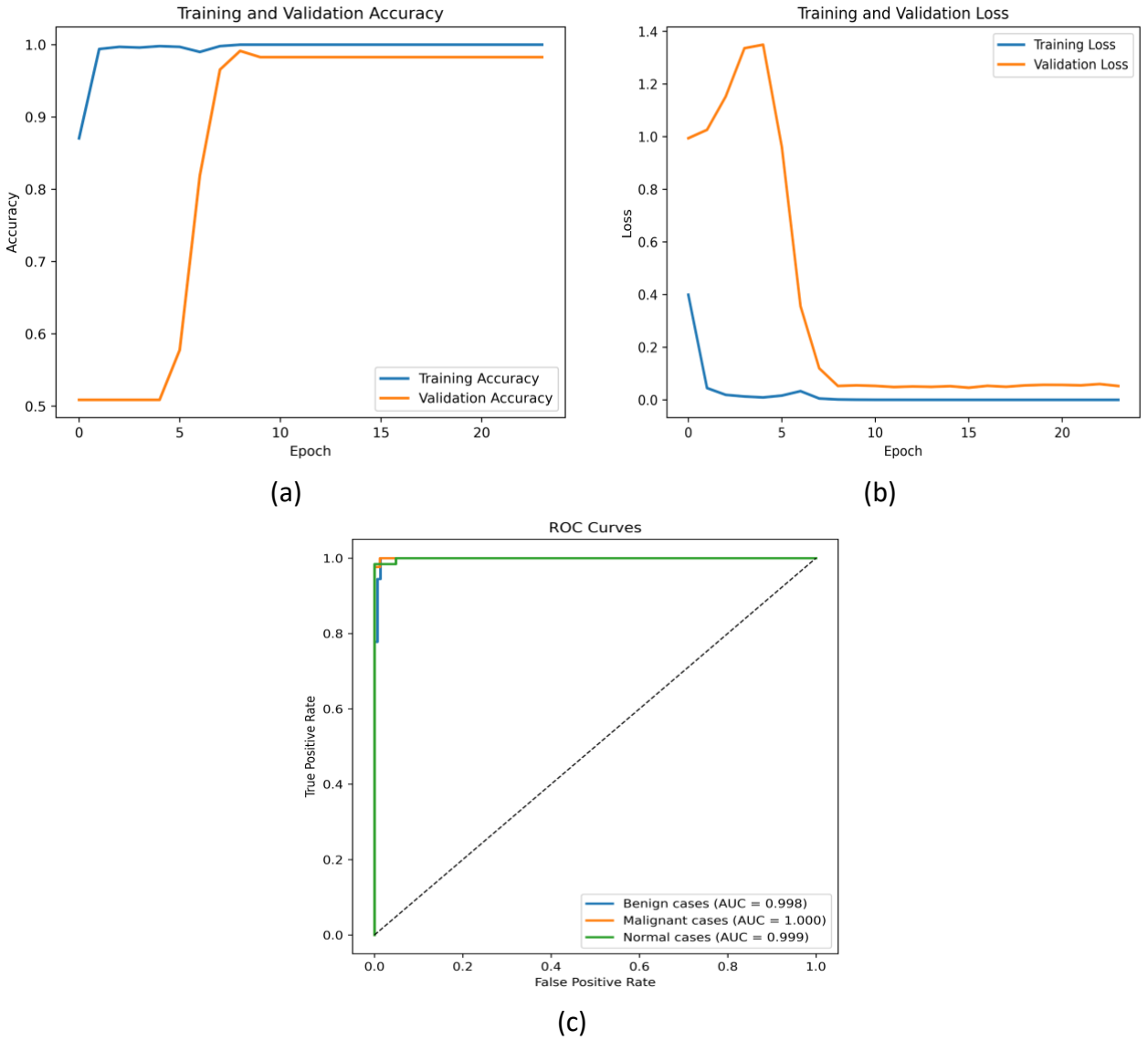

Fig. 5. Performance curve of the proposed model (a) Training and validation accuracy, (b) Training and validation loss, (c) ROC curves and AUC analysis.

Manuscript received 13 February 2026; Revised 10 April 2026; Accepted 12 April 2026; Available online 18 April 2026
Digital Object Identifier (**DOI**): https://doi.org/10.35882/jeeemi.v8i2.1574

discriminative capability across all classes. Cohen's Kappa coefficient was used to assess agreement between predicted and true labels. It achieved 96.88%, indicating excellent agreement beyond random chance. The receiver operating characteristic curves shown in Fig. 5(c) indicate the strong discriminative capability of the proposed LRSE-LCC model. Class-wise AUC values were 99.80% (benign), 100.00% (malignant), and 99.90% (normal), with a macro-averaged AUC of 99.90%. These results indicate excellent separability among the three categories. Further analysis using the normalized confusion matrix is shown in Fig. 6. The diagonal elements show that 89% of benign, 100% of malignant, and 98% of normal cases are correctly classified, indicating high true positive rates across all classes. The model achieves perfect classification for malignant cases with no false negatives, which is critical for clinical diagnosis. A small proportion of benign cases (6%) are misclassified as malignant, and normal, while 2% of normal cases are misclassified as benign. These misclassifications are primarily due to visual similarities between classes. The overall distribution confirms that the model maintains high classification accuracy with minimal error, as reflected by the low error rate of 1.81%.

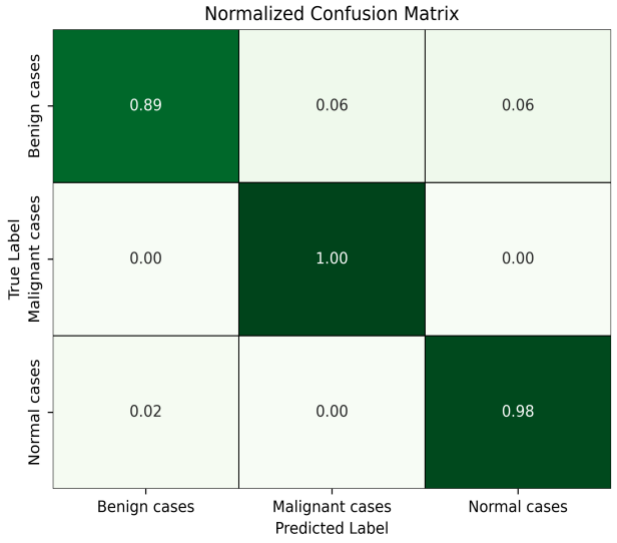

Fig. 6. Normalized Confusion matrix.

IV. Discussion

A. Performance comparison with state-of-the-art models

The performance of the proposed LRSE-LCC model is compared with various state-of-the-art methods published in the literature. These methods performed lung cancer detection and classification using the "IQ-OTH/NCCD" dataset. Table 3. summarizes this comparison. The comparison was done using various evaluation metrics, including accuracy, sensitivity, specificity, precision, AUC, F1-score and error rate [43]. Among these published methods, some achieved competitive model accuracy, including the UDCT model (96.82%), MobileNetV2-SGRU (96.83%), and the iSOA-based approach (96.58%). The proposed LRSE-LCC model achieved the highest accuracy of 98.19%, outperforming all comparative methods. The lightweight nature of the proposed LRSE-LCC model is supported by its low parameter count (~1.29 million). It is significantly smaller than many commonly used deep CNN architectures, which reduces computational complexity and memory requirements. This compact design makes the model particularly suitable for deployment in resource-constrained environments. Moreover, the model effectively learns discriminative features from CT images while maintaining robust generalization performance. This is also reflected in the stable training and validation trends shown in Fig. 5(b). Sensitivity is an important performance measure for clinical screening tasks. The LRSE-LCC model attained a sensitivity of 100.00%, performing better than all other competing approaches. This result indicates that no malignant samples were misclassified, which is highly significant in clinical settings. It ensures accurate identification of all cancer cases, facilitating early diagnosis and treatment, thereby improving patient outcomes and reducing the risk of misdiagnosis. The classification report further confirms the strong recall performance for malignant cases. Certain approaches, namely UDCT and SVM-Gabor-GLCM (Poly), attained a comparable sensitivity of 97.50% and 97.14%, respectively. The proposed LRSE-LCC model maintains a balance between sensitivity, accuracy, and error rates. This is very important for medical diagnosis tasks, where it is necessary to minimize the number of missed cancer cases while avoiding high false alarms.

Higher specificity always implies fewer false alarms, which in turn avoids unnecessary follow-ups and anxiety for patients. Certain approaches, namely UDCT and DeepNodule-Detect, attained a comparable specificity of 98.40% and 97.09%, respectively. Certain approaches, such as CNN (Google AI Studio), attained a significantly lower specificity of 76.40%, indicating their poor validity for use in practical clinical settings. The proposed LRSE-LCC model attained the highest specificity of 99.04%, performing better than all other competing approaches. The relatively low rate of false positives (0.96%) may require additional follow-up investigations and increase patient anxiety. However, as illustrated in Fig. 6, the confusion matrix shows that most predictions are correct, and the trade-off remains

Manuscript received 13 February 2026; Revised 10 April 2026; Accepted 12 April 2026; Available online 18 April 2026
Digital Object Identifier (**DOI**): https://doi.org/10.35882/jeeemi.v8i2.1574

acceptable in clinical scenarios where missing malignant cases is more critical. A detailed comparison shown in TABLE 3. and Fig. 7. indicates that while several existing models achieve competitive performance in specific evaluation metrics, they often exhibit trade-offs between accuracy, sensitivity, and computational complexity. For example, the UDCT model achieves slightly higher precision (98.70%) and F1-score (98.24%) compared to the proposed LRSE-LCC model. However, it has lower overall accuracy (96.82%) and a higher error rate (3.18%). This highlights a trade-off where improvements in certain metrics may come at the cost of overall classification performance. In contrast, the proposed LRSE-LCC model achieves the highest accuracy (98.19%) along with perfect sensitivity (100.00%), ensuring that no malignant cases are misclassified. This is particularly important in clinical diagnosis, where missing cancer cases can have serious consequences. Additionally, the model maintains high specificity (99.04%) and a low error rate (1.81%), demonstrating balanced, reliable performance across all evaluation metrics. Furthermore, unlike many deep CNN-based approaches, the proposed model maintains a lightweight architecture with approximately 1.29 million parameters, significantly reducing computational complexity. This makes it more suitable for deployment in real-world clinical environments where computational resources may be limited. Overall, the proposed LRSE-LCC model provides a better balance between accuracy, sensitivity, and efficiency compared to existing methods. The proposed LRSE-LCC model achieved an AUC of 99.90%, surpassing all comparative methods. Some of the comparative methods, including MobileNetV2-SGRU and CNN-based approaches, such as Google AI Studio, achieved (95.82%) and (82.40%). Several comparative methods did not report AUC values, which limits a comprehensive evaluation of class separability across different approaches. In contrast, the proposed LRSE-LCC model reports high AUC values for all classes, demonstrating its strong discriminative capability. Furthermore, the Cohen's kappa coefficient of 96.88% indicates almost perfect agreement between predicted and true class labels beyond chance, highlighting the robustness and reliability of the proposed LRSE-LCC model.

Overall, the comparative analysis shows that certain methods perform well on specific parameters, but the proposed LRSE-LCC framework achieves superior or competitive performance across all key evaluation parameters. The proposed method is more suitable for reliable lung cancer classification systems due to its ability to optimize all the parameters of evaluation simultaneously. Although statistical significance testing was not performed, consistent performance across 5-fold cross-validation, with a low standard deviation, indicates stable and reliable model behavior. A detailed statistical comparison will be considered in future work.

B. Limitations

Table 3. Performance Comparison of the Proposed LRSE-LCC Model and State-of-the-Art Methods

Methods	Evaluation Parameters (%)						
	Accuracy	Precision	Sensitivity	Specificity	F1-Score	AUC	Error
LRSE-LCC (Proposed)	**98.19**	97.00	**100.00**	**99.04**	96.42	**99.90**	**1.81**
UDCT [20]	96.82	**98.70**	97.50	98.40	**98.24**	-	3.18
iSOA Algorithm [15]	96.58	84.16	95.38	94.08	91.53	-	3.42
MobileNetV2-SGRU [23]	96.83	96.78	96.83	-	96.78	95.82	3.17
Modified Mask R-CNN (CBAM) [21]	-	92.60	90.10	-	-	-	-
CNN (Google AI Studio) [27]	75.50	-	74.50	76.40	-	82.40	24.50
DeepNodule-Detect [46]	95.43	-	93.40	97.09	-	-	4.57
CNN with AlexNet [26]	93.55	97.10	95.71	95.00	96.40	-	6.45
GoogLeNet TL [24]	94.38	-	95.08	93.70	-	-	5.62
SVM-Gabor-GLCM (Poly) [28]	89.89	98.55	97.14	97.50	97.84	-	10.11

Manuscript received 13 February 2026; Revised 10 April 2026; Accepted 12 April 2026; Available online 18 April 2026
Digital Object Identifier (**DOI**): https://doi.org/10.35882/jeeemi.v8i2.1574

Despite the excellent performance that has been achieved by the proposed LRSE-LCC framework, there are some limitations that should be pointed out. The study focuses on image-level classification and does not consider lesion-level localization, which could further improve the interpretability of the results. Though the framework has promising discriminative ability, the study can be further extended to consider the integration of explainable AI, as the importance of explainable deep learning frameworks in lung cancer detection from CT scans has been demonstrated in recent studies [44]. The integration of interpretable artificial intelligence in radiology is increasingly recognized as essential for enhancing clinical trust and adoption [45]. Furthermore, the "IQ-OTH/NCCD" dataset may have some inherent limitations in terms of demographic distribution and imaging conditions. It may have variations in scanner types and acquisition protocols. Such factors may impact the generalization capability of the proposed model in other clinical environments.

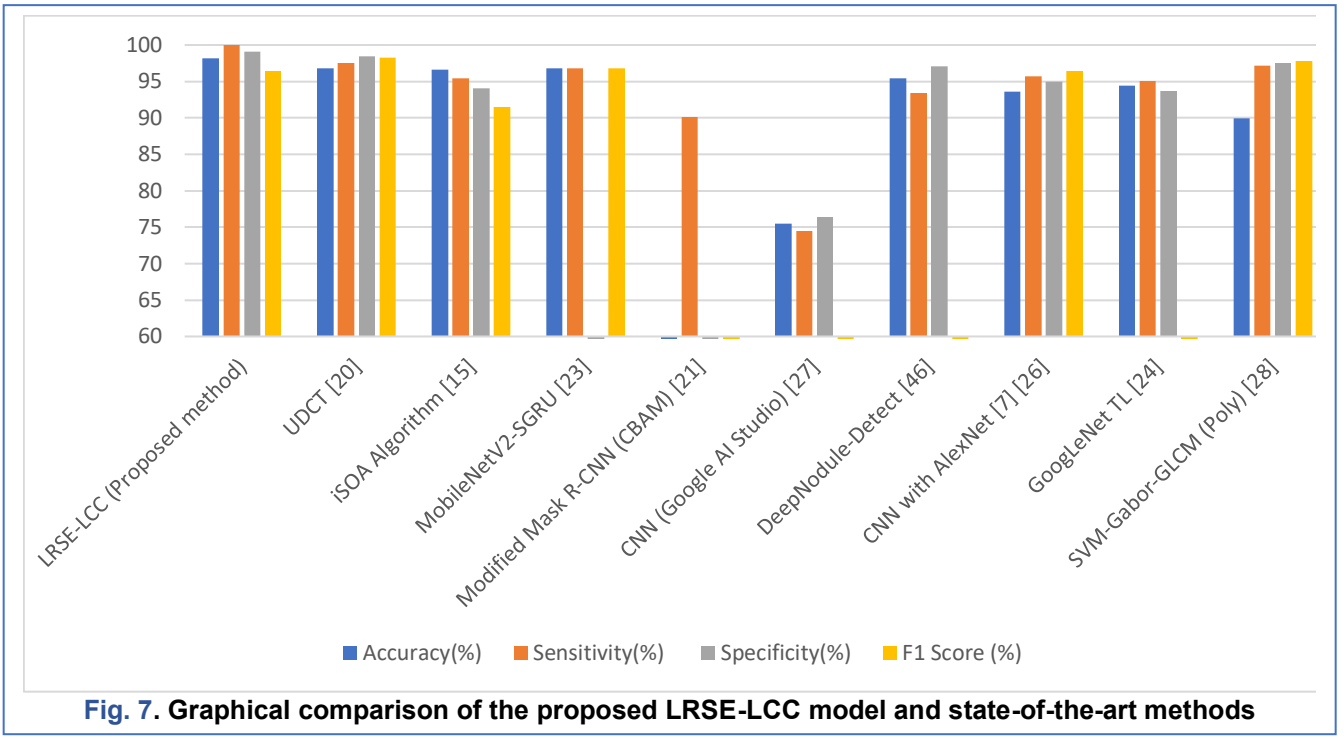

Fig. 7. Graphical comparison of the proposed LRSE-LCC model and state-of-the-art methods

V. Conclusion

This study introduced LRSE-LCC, a lightweight deep learning framework for lung cancer classification from CT images. The architecture combines residual connections with Squeeze-and-Excitation attention to enhance channel-wise feature learning while maintaining computational efficiency. Preprocessing, balanced batch training, and residual SE-based feature extraction contribute to stable training and improved generalization. In addition, the use of dual global pooling strengthens global contextual representation prior to classification. Experimental evaluation on the IQ-OTH/NCCD dataset demonstrates that LRSE-LCC achieves strong performance with a low error rate. Specifically, the model achieved accuracies of 100%, 98.28%, and 98.19% on the training, validation, and testing sets, respectively, with an overall error rate of 1.81%. The model also attained a macro-average precision of 97.00%, recall of 96.00%, and F1-score of 96.00%, while the weighted F1-score reached 98.00%. The Cohen's Kappa coefficient of 96.88% further confirms the robustness and reliability of the proposed approach. The model effectively captures discriminative imaging features while preserving a compact structure compared to conventional deep architectures. Overall, LRSE-LCC provides an efficient and reliable solution for automated lung cancer classification. Its lightweight design supports practical integration into computer-aided diagnostic systems. Future work will focus on extending the proposed framework to lesion-level analysis for precise localization of lung nodules, as well as incorporating explainable AI techniques (e.g., Grad-CAM) to enhance model interpretability. These directions aim to address the current limitations and improve clinical applicability in real-world diagnostic settings.

Acknowledgment

The authors acknowledge the creators of the "IQ-OTH/NCCD" dataset for providing open access to the

Manuscript received 13 February 2026; Revised 10 April 2026; Accepted 12 April 2026; Available online 18 April 2026
Digital Object Identifier (**DOI**): https://doi.org/10.35882/jeeemi.v8i2.1574

data, which enabled the development and evaluation of the proposed model.

Funding
No funds from public, private, or nonprofit organizations were used for this work.

Data Availability
The dataset used in this work is openly accessible.

Author Contribution
Dhaval Rana contributed to the conceptualization of the study, the design and development of the methodology, drafted the initial manuscript, and performed the experimental analysis. Keyur Rana contributed to the critical review of the manuscript and overall supervision of the research. All authors have reviewed and approved the final manuscript.

Declarations
Ethical Approval
Ethical approval was not required for this study, as it utilized a publicly available anonymized dataset.

Consent for Publication Participants.
Not applicable.

Competing Interests
The authors declare that they have no competing interests.

References
[1] World Health Organization, "Lung cancer," World Health Organization, Geneva, Switzerland, 2025. [Online]. Available: https://www.who.int/news-room/fact-sheets/detail/lung-cancer

[2] R. Sharma, "Mapping of global, regional and national incidence, mortality and mortality-to-incidence ratio of lung cancer in 2020 and 2050," *Int. J. Clin. Oncol.*, vol. 27, no. 4, pp. 665–675, 2022, doi: 10.1007/s10147-021-02108-2.

[3] American Cancer Society, "Key statistics for lung cancer," American Cancer Society, Atlanta, GA, USA, 2025. [Online]. Available: https://www.cancer.org/cancer/types/lung-cancer.html.

[4] International Agency for Research on Cancer, "Cancer incidence and mortality worldwide: GLOBOCAN 2022," IARC, Lyon, France, 2022. [Online].Available: https://gco.iarc.who.int/today/en/dataviz/bars

[5] G. C. Forte *et al.*, "Deep Learning Algorithms for Diagnosis of Lung Cancer: A Systematic Review and Meta-Analysis," *Cancers (Basel).*, vol. 14, no. 16, pp. 1–11, 2022, doi: 10.3390/cancers14163856.

[6] X. Chen *et al.*, "Recent advances and clinical applications of deep learning in medical image analysis," *Med. Image Anal.*, vol. 79, p. 102444, 2022, doi: 10.1016/j.media.2022.102444.

[7] H. Wang, H. Zhu, L. Ding, and K. Yang, "A diagnostic classification of lung nodules using multiple-scale residual network," *Sci. Rep.*, vol. 13, no. 1, pp. 1–11, 2023, doi: 10.1038/s41598-023-38350-z.

[8] M. Singh and M. K. Singh, "Content based medical image retrieval using deep learning and handcrafted features in dimensionality reduction framework," *Comput. Electr. Eng.*, vol. 127, no. PA, p. 110581, 2025, doi: 10.1016/j.compeleceng.2025.110581.

[9] K. He, X. Zhang, S. Ren, and J. Sun, "Deep residual learning for image recognition," *Proc. IEEE Comput. Soc. Conf. Comput. Vis. Pattern Recognit.*, vol. 2016-Decem, pp. 770–778, 2016, doi: 10.1109/CVPR.2016.90.

[10] G. Huang, Z. Liu, L. Van Der Maaten, and K. Q. Weinberger, "Densely connected convolutional networks," *Proc. - 30th IEEE Conf. Comput. Vis. Pattern Recognition, CVPR 2017*, vol. 2017-Janua, pp. 2261–2269, 2017, doi: 10.1109/CVPR.2017.243.

[11] M. Tan and Q. V. Le, "EfficientNet: Rethinking Model Scaling for Convolutional Neural Networks," May 2019, Accessed: Dec. 21, 2023. [Online]. Available: http://arxiv.org/abs/1905.11946

[12] M. Li, Y. Jiang, Y. Zhang, and H. Zhu, "Medical image analysis using deep learning algorithms," *Front. Public Heal.*, vol. 11, no. November, pp. 1–28, 2023, doi: 10.3389/fpubh.2023.1273253.

[13] H. Kadara *et al.*, "Early diagnosis and screening for lung cancer," *Cold Spring Harb. Perspect. Med.*, vol. 11, no. 9, pp. 1–20, 2021, doi: 10.1101/cshperspect.a037994.

[14] I. Ahmed, A. Chehri, G. Jeon, and F. Piccialli, "Automated Pulmonary Nodule Classification and Detection Using Deep Learning Architectures," *IEEE/ACM Trans. Comput. Biol. Bioinforma.*, vol. 20, no. 4, pp. 2445–2456, 2023, doi: 10.1109/TCBB.2022.3192139.

[15] C. Yan and N. Razmjooy, "Optimal lung cancer detection based on CNN optimized and improved Snake optimization algorithm," *Biomed. Signal Process. Control*, vol. 86, Sep. 2023, doi: 10.1016/j.bspc.2023.105319.

Manuscript received 13 February 2026; Revised 10 April 2026; Accepted 12 April 2026; Available online 18 April 2026
Digital Object Identifier (**DOI**): https://doi.org/10.35882/jeeemi.v8i2.1574

[16] Y. Xu, Y. Wang, and N. Razmjooy, "Lung cancer diagnosis in CT images based on Alexnet optimized by modified Bowerbird optimization algorithm," *Biomed. Signal Process. Control*, vol. 77, no. April, p. 103791, 2022, doi: 10.1016/j.bspc.2022.103791.

[17] A. A. Abe, M. Nyathi, A. A. Okunade, W. Pilloy, B. Kgole, and N. Nyakale, "A robust deep learning algorithm for lung cancer detection from computed tomography images," *Intell. Med.*, vol. 11, no. January, p. 100203, 2025, doi: 10.1016/j.ibmed.2025.100203.

[18] W. Li *et al.*, "Machine Learning Model of ResNet50-Ensemble Voting for Malignant–Benign Small Pulmonary Nodule Classification on Computed Tomography Images," *Cancers (Basel).*, vol. 15, no. 22, 2023, doi: 10.3390/cancers15225417.

[19] M. Celik and O. Inik, "Review of deep learning-based segmentation methods: Popular approaches, literature gaps, and opportunities," *Displays*, vol. 91, no. October 2025, p. 103225, 2026, doi: 10.1016/j.displa.2025.103225.

[20] A. Gupta, A. Kumar, and K. Rautela, "UDCT: lung Cancer detection and classification using U-net and DARTS for medical CT images," *Multimed. Tools Appl.*, vol. 84, no. 18, pp. 19065–19085, 2025, doi: 10.1007/s11042-024-19801-9.

[21] K. V. Aishwarya, A. Asuntha, and J. Murugan, *Optimizing pulmonary nodule segmentation in CT imaging: A comparative study of anchor-based and anchor-free detectors using attention mechanism*, vol. 84, no. 32. Springer US, 2025. doi: 10.1007/s11042-025-20752-y.

[22] S. Aslani *et al.*, "Enhancing cancer prediction in challenging screen-detected incident lung nodules using time-series deep learning," *Comput. Med. Imaging Graph.*, vol. 116, no. March, 2024, doi: 10.1016/j.compmedimag.2024.102399.

[23] A. Bagheri Tofighi, A. Ahmadi, and H. Mosadegh, "Improving lung cancer detection via MobileNetV2 and stacked-GRU with explainable AI," *Int. J. Inf. Technol.*, vol. 17, no. 2, pp. 1189–1196, 2025, doi: 10.1007/s41870-024-02045-z.

[24] M. S. AL-Huseiny and A. S. Sajit, "Transfer learning with GoogLeNet for detection of lung cancer," *Indones. J. Electr. Eng. Comput. Sci.*, vol. 22, no. 2, pp. 1078–1086, 2021, doi: 10.11591/ijeecs.v22.i2.pp1078-1086.

[25] A. Saha, S. M. Ganie, P. K. D. Pramanik, R. K. Yadav, S. Mallik, and Z. Zhao, "VER-Net: a hybrid transfer learning model for lung cancer detection using CT scan images," *BMC Med. Imaging*, vol. 24, no. 1, pp. 1–18, 2024, doi: 10.1186/s12880-024-01238-z.

[26] H. F. Al-Yasriy, M. S. AL-Husieny, F. Y. Mohsen, E. A. Khalil, and Z. S. Hassan, "Diagnosis of Lung Cancer Based on CT Scans Using CNN," *IOP Conf. Ser. Mater. Sci. Eng.*, vol. 928, no. 2, p. 22035, Nov. 2020, doi: 10.1088/1757-899X/928/2/022035.

[27] Z. Aljneibi, S. Almenhali, and L. Lanca, "Convolutional neural network application for automated lung cancer detection on chest CT using Google AI Studio," *Radiography*, vol. 31, 2025, doi: 10.1016/j.radi.2025.103152.

[28] H. F. Kareem, M. S. AL-Husieny, F. Y. Mohsen, E. A. Khalil, and Z. S. Hassan, "Evaluation of SVM performance in the detection of lung cancer in marked CT scan dataset," *Indones. J. Electr. Eng. Comput. Sci.*, vol. 21, no. 3, pp. 1731–1738, 2021, doi: 10.11591/ijeecs.v21.i3.pp1731-1738.

[29] S. Aslani *et al.*, "Enhancing cancer prediction in challenging screen-detected incident lung nodules using time-series deep learning," *Comput. Med. Imaging Graph.*, vol. 116, no. October 2023, 2024, doi: 10.1016/j.compmedimag.2024.102399.

[30] M. Nasir, M. S. Farid, Z. Suhail, and M. H. Khan, "Optimal Thresholding for Multi-Window Computed Tomography (CT) to Predict Lung Cancer," *Appl. Sci.*, vol. 13, no. 12, 2023, doi: 10.3390/app13127256.

[31] S. Tang, R. Ma, Q. Li, Y. Bai, and S. Chen, "Classification of Benign and Malignant Pulmonary Nodules Based on the Multiresolution 3D DPSECN Model and Semisupervised Clustering," *IEEE Access*, vol. 9, pp. 43397–43410, 2021, doi: 10.1109/ACCESS.2021.3060178.

[32] I. W. Harsono, S. Liawatimena, and T. W. Cenggoro, "Lung nodule detection and classification from Thorax CT-scan using RetinaNet with transfer learning," *J. King Saud Univ. - Comput. Inf. Sci.*, vol. 34, no. 3, pp. 567–577, 2022, doi: 10.1016/j.jksuci.2020.03.013.

[33] S. R. Jena, S. T. George, and D. N. Ponraj, "Lung cancer detection and classification with DGMM-RBCNN technique," *Neural Comput. Appl.*, vol. 33, no. 22, pp. 15601–15617, 2021, doi: 10.1007/s00521-021-06182-5.

[34] S. Zheng *et al.*, "Deep convolutional neural networks for multiplanar lung nodule detection: Improvement in small nodule identification," *Med. Phys.*, vol. 48, no. 2, pp. 733–744, 2021, doi: 10.1002/mp.14648.

Manuscript received 13 February 2026; Revised 10 April 2026; Accepted 12 April 2026; Available online 18 April 2026
Digital Object Identifier (**DOI**): https://doi.org/10.35882/jeeemi.v8i2.1574

[35] H. Mkindu, L. Wu, and Y. Zhao, "Lung nodule detection in chest CT images based on vision transformer network with Bayesian optimization," *Biomed. Signal Process. Control*, vol. 85, no. January, p. 104866, 2023, doi: 10.1016/j.bspc.2023.104866.

[36] A. A. Shah, H. A. M. Malik, A. H. Muhammad, A. Alourani, and Z. A. Butt, "Deep learning ensemble 2D CNN approach towards the detection of lung cancer," *Sci. Rep.*, vol. 13, no. 1, pp. 1–15, 2023, doi: 10.1038/s41598-023-29656-z.

[37] B. A.R., V. K. R.S., and K. S.S., "LCD-Capsule Network for the Detection and Classification of Lung Cancer on Computed Tomography Images," *Multimed. Tools Appl.*, vol. 82, no. 24, pp. 37573–37592, 2023, doi: 10.1007/s11042-023-14893-1.

[38] J. Hu, L. Shen, S. Albanie, G. Sun, and E. Wu, "Squeeze-and-Excitation Networks," *IEEE Trans. Pattern Anal. Mach. Intell.*, vol. 42, no. 8, pp. 2011–2023, 2020, doi: 10.1109/TPAMI.2019.2913372.

[39] alyasriy, hamdalla, AL-Huseiny, and Muayed, "The IQ-OTH/NCCD lung cancer dataset," 2023, *Mendeley Data*. doi: http://doi.org/10.17632/bhmdr45bh2.4.

[40] D. Singh and B. Singh, "Investigating the impact of data normalization on classification performance," *Appl. Soft Comput.*, vol. 97, p. 105524, 2020, doi: https://doi.org/10.1016/j.asoc.2019.105524.

[41] A. Zafar *et al.*, "A Comparison of Pooling Methods for Convolutional Neural Networks," *Appl. Sci.*, vol. 12, no. 17, pp. 1–21, 2022, doi: 10.3390/app12178643.

[42] S. A. Zaidi, V. Chouvatut, C. Phongnarisorn, and D. Praserttitipong, "Deep learning based detection of endometriosis lesions in laparoscopic images with 5-fold cross-validation," *Intell. Med.*, vol. 11, no. January, p. 100230, 2025, doi: 10.1016/j.ibmed.2025.100230.

[43] D. M. Ibrahim, N. M. Elshennawy, and A. M. Sarhan, "Deep-chest: Multi-classification deep learning model for diagnosing COVID-19, pneumonia, and lung cancer chest diseases," *Comput. Biol. Med.*, vol. 132, May 2021, doi: 10.1016/j.compbiomed.2021.104348.

[44] C. Mello-Thoms and C. A. B. Mello, "AI IN IMAGING AND THERAPY: INNOVATIONS, ETHICS, AND IMPACT: REVIEW ARTICLE Clinical applications of artificial intelligence in radiology," *Br. J. Radiol.*, vol. 96, no. 1150, 2023, doi: 10.1259/bjr.20221031.

[45] M. Hammad, M. ElAffendi, A. A. A. El-Latif, A. A. Ateya, G. Ali, and P. Plawiak, "Explainable AI for lung cancer detection via a custom CNN on CT images," *Sci. Rep.*, vol. 15, no. 1, pp. 1–21, 2025, doi: 10.1038/s41598-025-97645-5.

[46] A. A. Abe, M. Nyathi, A. A. Okunade, W. Pilloy, B. Kgole, and N. Nyakale, "A robust deep learning algorithm for lung cancer detection from computed tomography images," *Intell. Med.*, vol. 11, p. 100203, 2025, doi: https://doi.org/10.1016/j.ibmed.2025.100203.

Author Biography

Mr. Dhaval J. Rana received his Bachelor of Engineering degree in Computer Engineering from Gujarat University, Gujarat, India, in 2011, and his Master of Engineering degree in Information Technology from Gujarat Technological University, Gujarat, India, in 2013. He is currently pursuing his Ph.D. degree at Gujarat Technological University. He is presently working as an Assistant Professor in the Department of Artificial Intelligence and Data Science at Sarvajanik College of Engineering and Technology, Surat, India. He has a total of twelve years of teaching experience in higher education. His research interests include artificial intelligence, machine learning, and wireless sensor networks, reflecting his focus on emerging technologies and intelligent computing applications within the domain of computer engineering.

Dr. Keyur Rana received his Ph.D. degree in Computer Engineering from Sardar Vallabhbhai National Institute of Technology, Surat, India. He is currently a Professor in the Department of Computer Engineering at Sarvajanik College of Engineering and Technology, Surat, India, and also serves as Pro-Dean, Faculty of Engineering. He has a total of 27 years of experience in teaching at the Undergraduate and Postgraduate levels, research, and academic administration. His fields of specialization include machine learning and deep learning. He has presented at various reputable international conferences and published several research papers in peer-reviewed journals.

Manuscript received 13 February 2026; Revised 10 April 2026; Accepted 12 April 2026; Available online 18 April 2026
Digital Object Identifier (**DOI**): https://doi.org/10.35882/jeeemi.v8i2.1574

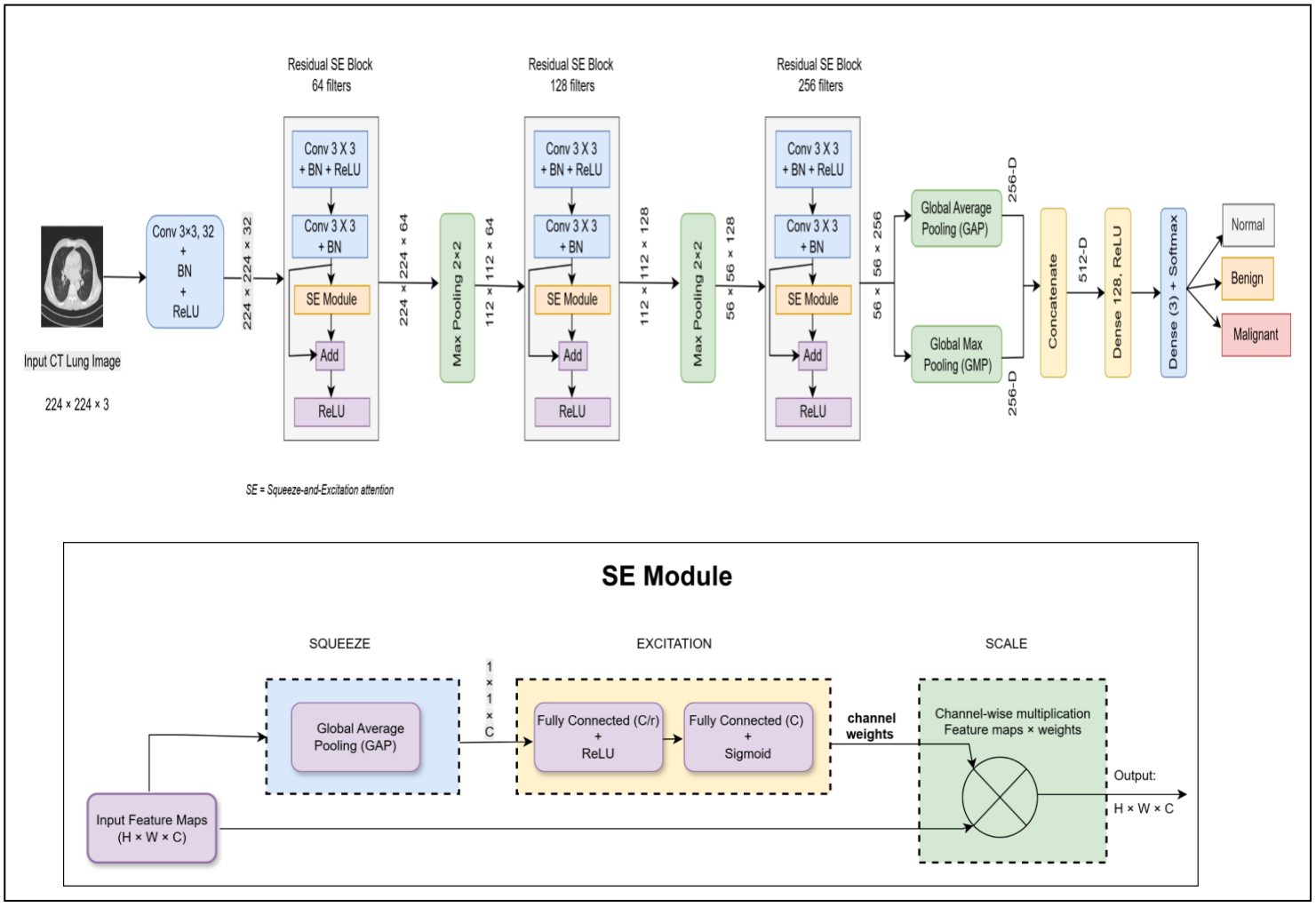

Manuscript received 13 February 2026; Revised 10 April 2026; Accepted 12 April 2026; Available online 18 April 2026
Digital Object Identifier (**DOI**): https://doi.org/10.35882/jeeemi.v8i2.1574